

A MODEL OF MACROSCALE DEFORMATION AND MICROVIBRATION IN SKELETAL MUSCLE TISSUE

BERND SIMEON¹, RADU SERBAN² AND LINDA R. PETZOLD³

Abstract. This paper deals with modelling the passive behavior of skeletal muscle tissue including certain microvibrations at the cell level. Our approach combines a continuum mechanics model with large deformation and incompressibility at the macroscale with chains of coupled nonlinear oscillators. **The model verifies that an externally applied vibration at the appropriate frequency is able to synchronize microvibrations in skeletal muscle cells.** From the numerical analysis point of view, one faces here a partial differential-algebraic equation (PDAE) that after semi-discretization in space by finite elements possesses an index up to three, depending on certain physical parameters. In this context, the consequences for the time integration as well as possible remedies are discussed.

Résumé. ...

1991 Mathematics Subject Classification. 65L05, 65L80, 65M12, 65M20, 74C05.

September 27, 2008.

INTRODUCTION

Complex biological systems exhibit a great variety of phenomena that demand for appropriate mathematical models and corresponding numerical simulation methods. **In this contribution, we focus on the dynamics of skeletal muscle tissue and introduce a top-down approach that combines a continuum mechanics model at the macroscopic level with clusters of oscillating cells at the microscopic level.** From a mathematical viewpoint, this approach leads to a coupled system of transient PDEs and ODEs, which after semi-discretization in space by finite elements turns out to be a system of index three DAEs [1].

Dating back to Hill [14] and Huxley [16], skeletal muscles have been the subject of extensive research for several decades. **A variety of models exist [18] that can be classified in terms of biological structure, i.e., at the tissue, cell or intra-cellular scale, or in terms of mathematical properties, i.e., discrete versus continuous models.** Due to limited resources and an insufficient understanding of mutual coupling mechanisms between different levels, however, most computational approaches have so far tended to target a relatively narrow section of this model hierarchy.

A new aspect comes into play when the microvibration of skeletal muscle cells is taken into account. This phenomenon is related to physiological tremor and features also similarities to the rhythmic excitation of cardiac cells [9]. The absence of these microvibrations in outer space missions [8] as well as in cancerous tissue indicates

Keywords and phrases: skeletal muscle tissue, microvibrations, coherence, PDAE, index, time integration

¹ Zentrum Mathematik, TU München, Boltzmannstr. 3, 85748 Garching, Germany

² Xulu entertainment 890 Hillview Court, Milpitas, CA 95032

³ Dept. of Mechanical Engineering, University of California Santa Barbara, CA 93106, USA

their relevance for physiological transport processes in the extracellular matrix structure. New therapy concepts mechanically stimulate the diseased muscle tissue and lead to a synchronization effect, also called entrainment [21]. A detailed model of the driving mechanisms based on specific parameters such as ion concentration, base-acid content or osmolarity has not been available so far.

Our goal here is to develop a simple mechanical model for the cell's microvibrations and to demonstrate how it can be coupled with a macroscopic PDE model for the muscle tissue. The ultimate vision is to be able to predict the dynamics of vibrational therapies so that the validity of the underlying physiological assumptions can be tested. On this road towards a realistic multi-level model, we present the first steps and also a methodology that should be open to further extensions in the direction of systems biology. An important feature of the model is that it can be expressed directly in the COMSOL framework [5], giving access to COMSOL's libraries of material properties and models, and the ability to extend to complex geometries and multiphysics. Thus the model is open towards an incorporation of greater physical or physiological details.

With respect to the underlying mathematical structures, our approach features some parallels to the Bidomain equations for the electrical activity of the heart [17]. There one has also a coupled system with a continuum model that describes the spatial distribution of the trans-membrane potential and a set of ODEs for physiological parameters such as ionic fluxes and enzyme kinetics. For the computational treatment of the PDE part, the usage of the finite element method is first choice as complicated geometries need to be resolved. The system of semi-discretized Bidomain equations forms also a DAE, but the index is one instead of three, as in our case where the higher index results from the equations of incompressible elasticity that are typically required to model muscle tissue. A closer look at the equations, however, reveals that actually the incompressibility constraint is weakened by a regularization term, which in turn represents a singular perturbation.

The microvibrations at the cell level are modelled in terms of a one-dimensional chain of oscillators that corresponds to an appropriate one-dimensional cross-section through the tissue. The oscillators possess a nonlinearity of Van der Pol type. As one of the objectives of the modeling is to determine whether an externally-driven microvibration applied to the muscle tissue can cause synchronization of the cellular oscillators, we introduce a measure of synchronization, the coherence, and record it along the simulation runs.

This paper is organized as follows: In Section 1 we introduce a constrained nonlinear PDE model of the macroscopic skeletal muscle tissue along with an ODE model of the microscale oscillating cells. We then discuss these models and their coupling. In Section 2 we examine the structure of the semi-discretized PDAE model, showing that depending on the parameters, the index can be up to three. Furthermore, we apply index reduction and explore alternative formulations to obtain a more reliable and efficient time integration. It turns out that a straightforward stabilized index-two formulation in the PDE context may lead to an incorrect implementation using COMSOL defaults. Numerical simulations illustrating the synchronization of the oscillators and the results of the two-dimensional PDE model are presented in Section 3. Section 4 concludes with a summary of the results and a discussion of future directions.

1. SKELETAL MUSCLE TISSUE MODEL

The behavior of skeletal muscles at the macroscale is typically described by biomechanical models that are related to the equations of multibody dynamics and deformable bodies. Probably the oldest approach is the model of Hill [14], which treats the muscle as a nonlinear force law with contracting element, serial elastic element, and parallel elastic element. It is still in wide use for biomechanical studies such as gait analysis that are based on a multibody representation.

At the microscale, the famous model of Huxley [16] describes the activation of muscle tissue by means of the cross-bridges between actin and myosin inside each cell. During muscle contraction, a fraction of these cross-bridges is attached and subsequently released. The distribution of attached cross-bridges satisfies a transport equation that is driven by external controls and the amount of available calcium in the myofibrillar space. Since the solution of this first order PDE at the cell level requires a substantial computational effort, reduced ODE models of the actin-myosin binding have been developed [25] that can be used in combination with continuum mechanics models.

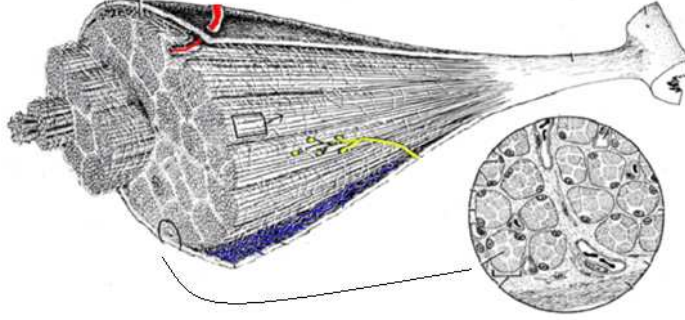


FIGURE 1. Skeletal muscle with detail of lateral cross section on the right

Fig. 1 shows a skeletal muscle with a detail of a lateral cross section. **The muscle cells form long fibres in longitudinal direction, and as the cross section reveals, the cells are arranged in a matrix-like structure, which is the extracellular matrix.** It consists mainly of different protein structures, in particular collagen.

In the following, we first deal with the macroscale by looking deeper into a standard continuum mechanics approach. Thereafter, the microscale is discussed.

1.1. A Model from Continuum Mechanics

Soft biological materials such as muscle tissue can be viewed as deformable bodies that possess a certain geometry and specific material parameters. Several aspects deserve particular attention in the development of a realistic model. The body may undergo large deformations and rigid body motions, the constitutive law relating stress and strain is nonlinear and often anisotropic, and the large fraction of water makes the material almost incompressible [11]. One also has to distinguish between active behavior, a contraction process controlled by the actin-myosin binding in each cell, and passive behavior, in which the muscle tissue changes solely due to external forces. In this work, we restrict ourselves to passive behavior and apply next a step by step procedure to establish the model equations at the macroscale. For a general treatment of elasticity theory see [19].

Linear Elasticity, Incompressible Case

We start with the small deformation case and consider a solid that occupies the spatial reference domain $\Omega \subset \mathbb{R}^3$. A material point in cartesian coordinates is denoted by $x \in \Omega$, and $t \in [0, T]$ stands for the time. The vector field $\mathbf{u}(x, t) \in \mathbb{R}^3$ is the displacement of the solid body.

Next, we introduce as usual the strain tensor

$$\boldsymbol{\varepsilon} = \boldsymbol{\varepsilon}(\mathbf{u}) = \frac{1}{2}(\nabla \mathbf{u} + \nabla \mathbf{u}^T) \quad (1)$$

where $\nabla = \partial/\partial x$, which can be viewed as a symmetric 3×3 Jacobian matrix of the displacement. Furthermore, we assume Hooke's law

$$\boldsymbol{\sigma} = \boldsymbol{\sigma}(\mathbf{u}) = \Lambda(\text{trace } \boldsymbol{\varepsilon}(\mathbf{u}))\mathbf{I} + 2\zeta\boldsymbol{\varepsilon}(\mathbf{u}) \quad (2)$$

for the relation between strain and stress tensor $\boldsymbol{\sigma}$, with 3×3 identity matrix \mathbf{I} and Lamé constants Λ and ζ as material parameters. Hooke's law will be extended below to the more general class of hyperelastic materials.

For Hooke's law, one may also formulate the strain energy as tensor product $\boldsymbol{\sigma} : \boldsymbol{\varepsilon} = \text{trace}(\boldsymbol{\sigma}\boldsymbol{\varepsilon})$ of stress and strain, integrated over the whole body,

$$W = \frac{1}{2} \int_{\Omega} \boldsymbol{\sigma} : \boldsymbol{\varepsilon} \, dx. \quad (3)$$

Frequently, one makes use of an alternative notation for Hooke's law that is based on a vector representation of the tensors $\boldsymbol{\sigma}$ and $\boldsymbol{\varepsilon}$. Set

$$\underline{\boldsymbol{\varepsilon}} := (\varepsilon_{11}, \varepsilon_{22}, \varepsilon_{33}, 2\varepsilon_{12}, 2\varepsilon_{23}, 2\varepsilon_{13})^T, \quad \underline{\boldsymbol{\sigma}} := (\sigma_{11}, \sigma_{22}, \sigma_{33}, \sigma_{12}, \sigma_{23}, \sigma_{13})^T$$

and replace the Lamé constants by Poisson's number $\nu = \Lambda/(2(\Lambda + \zeta))$ and modulus of elasticity $E = \zeta(3\Lambda + 2\zeta)/(\Lambda + \zeta)$. Hooke's law (2) then reads $\underline{\boldsymbol{\sigma}} = \mathbf{D} \underline{\boldsymbol{\varepsilon}}$ with constant 6×6 matrix

$$\mathbf{D} = \frac{E}{(1+\nu)(1-2\nu)} \begin{pmatrix} 1-\nu & \nu & \nu & & & \\ \nu & 1-\nu & \nu & & & \\ \nu & \nu & 1-\nu & & & \\ & & & (1-2\nu)/2 & & \\ & & & & (1-2\nu)/2 & \\ & & & & & (1-2\nu)/2 \end{pmatrix}. \quad (4)$$

As inspection of matrix \mathbf{D} shows, the case $\nu = \frac{1}{2}$, which in fact corresponds to incompressibility, deserves special attention. We will come back to that point in the next paragraph. For the moment, we put everything together by invoking the balance of momentum and summarize the equations of motion of linear elasticity in strong form as

$$\rho \ddot{\mathbf{u}}(x, t) = \mathbf{div} \boldsymbol{\sigma}(\mathbf{u}(x, t)) + \mathbf{f}(x, t) \quad \text{in } \Omega \quad (5)$$

where $\boldsymbol{\sigma}$ is given by Hooke's law (2) or (4), respectively. Furthermore, ρ is the mass density and \mathbf{f} the vector of internal loads.

Incompressibility

As pointed out above, for $\nu \rightarrow 1/2$ we are approaching the incompressible case where the equations (5) are not well-defined. Biological tissue consists to 70 % or more of water, which renders such materials not fully but almost incompressible. With respect to Poisson's number ν , this means that ν may assume a value between 0.45 up to 0.49. It is well-known that this may lead to problems such as locking and spatial oscillations with regard to the finite element approximation in space, and therefore one usually prefers a mixed formulation in such situations.

In order to set up a mixed formulation, we introduce the scalar pressure $p(x, t)$ as negative mean stress

$$p = -\frac{\sigma_{11} + \sigma_{22} + \sigma_{33}}{3} \quad (6)$$

depending on the normal stress components $\sigma_{11}, \sigma_{22}, \sigma_{33}$. Thus we may rewrite Hooke's law as

$$\underline{\boldsymbol{\sigma}} = \underline{\boldsymbol{\sigma}}(\mathbf{u}, p) = \mathbf{D}_d \underline{\boldsymbol{\varepsilon}} + (p, p, p, 0, 0, 0)^T \quad (7)$$

with deviatoric elasticity matrix \mathbf{D}_d . Moreover, a straightforward computation shows that the definition (6) of the pressure can be re-expressed as the constraint equation

$$\frac{p}{\kappa} + \varepsilon_{11} + \varepsilon_{22} + \varepsilon_{33} = 0 \quad (8)$$

with bulk modulus $\kappa = E/(3(1-2\nu))$. In the limit case $\nu \rightarrow \frac{1}{2}$, the bulk modulus obviously tends to infinity, which means that it may also be employed as a measure of the incompressibility as long as that limit situation is not reached.

The definitions of the divergence and of the strain tensor immediately imply

$$\varepsilon_{11} + \varepsilon_{22} + \varepsilon_{33} = \operatorname{div} \mathbf{u}.$$

In other words, incompressibility for solids leads to the same zero divergence constraint as incompressibility for fluids. In total, we thus end up with the equations of motion in the incompressible case

$$\begin{aligned} \rho \ddot{\mathbf{u}} - \operatorname{div} \boldsymbol{\sigma}(\mathbf{u}, p) &= \mathbf{f}, \\ \frac{p}{\kappa} + \operatorname{div} \mathbf{u} &= 0 \end{aligned} \quad \text{in } \Omega. \quad (9)$$

Finally, we apply one more transformation to obtain better insight into the structure of this PDE. Observe that according to (7), we can furthermore split the divergence of $\boldsymbol{\sigma}(\mathbf{u}, p)$ into

$$\operatorname{div} \boldsymbol{\sigma}(\mathbf{u}, p) = \operatorname{div} \boldsymbol{\sigma}_d(\mathbf{u}) + \nabla p,$$

with a deviatoric stress tensor $\boldsymbol{\sigma}_d$. In the limit $\nu \rightarrow 1/2$, one obtains

$$\begin{aligned} \rho \ddot{\mathbf{u}} - \operatorname{div} \boldsymbol{\sigma}_d(\mathbf{u}) - \nabla p &= \mathbf{f}, \\ \operatorname{div} \mathbf{u} &= 0 \end{aligned} \quad \text{in } \Omega$$

These equations of motion exhibit a similar structure as the Navier-Stokes equations in fluid dynamics. However, the second time derivative of the displacement is a major difference and affects the index of the DAE that results from spatial discretization, see Section 2 below.

Damping

Muscle tissue clearly features dissipative properties, and thus a reasonable model should include some kind of damping. We choose here the most widespread approach, which is Rayleigh damping. Instead of Hooke's law (2), one assumes in this case the stress-strain relation

$$\tilde{\boldsymbol{\sigma}} = \Lambda(\operatorname{trace} \boldsymbol{\varepsilon}(\mathbf{u} + \beta \dot{\mathbf{u}})) \mathbf{I} + 2\zeta \boldsymbol{\varepsilon}(\mathbf{u} + \beta \dot{\mathbf{u}}) = \boldsymbol{\sigma}(\mathbf{u}) + \beta \frac{d}{dt} \boldsymbol{\sigma}(\mathbf{u}). \quad (10)$$

The parameter $\beta \geq 0$ specifies damping depending on the body's frequencies. With a second parameter $\alpha \geq 0$ determining viscous damping, the equations of motion (5) are then rewritten as

$$\rho(\ddot{\mathbf{u}} + \alpha \dot{\mathbf{u}}) = \operatorname{div} \boldsymbol{\sigma}(\mathbf{u}) + \beta \operatorname{div} \frac{d}{dt} \boldsymbol{\sigma}(\mathbf{u}) + \mathbf{f} \quad \text{in } \Omega. \quad (11)$$

Note that (11) refers to the standard formulation in the compressible case. For the mixed formulation with the pressure as second variable, the frequency-dependent damping term becomes

$$\tilde{\boldsymbol{\sigma}} = \boldsymbol{\sigma}(\mathbf{u}, p) + \beta \frac{d}{dt} \boldsymbol{\sigma}(\mathbf{u}, p) = \boldsymbol{\sigma}(\mathbf{u}, p) + \beta \boldsymbol{\sigma}(\dot{\mathbf{u}}, \dot{p}).$$

As the stress-strain relation is linear, the differentiation with respect to time goes directly through to the displacement field and the pressure.

Summing up, the equations of motion including incompressibility and damping yield

$$\begin{aligned} \rho(\ddot{\mathbf{u}} + \alpha \dot{\mathbf{u}}) - \operatorname{div} \boldsymbol{\sigma}(\mathbf{u}, p) - \beta \operatorname{div} \boldsymbol{\sigma}(\dot{\mathbf{u}}, \dot{p}) &= \mathbf{f}, \\ \frac{p}{\kappa} + \operatorname{div} \mathbf{u} &= 0 \end{aligned} \quad \text{in } \Omega. \quad (12)$$

Using the splitting for the stress tensor as discussed above, this is equivalent to

$$\begin{aligned} \rho(\ddot{\mathbf{u}} + \alpha \dot{\mathbf{u}}) - \operatorname{div} \boldsymbol{\sigma}_d(\mathbf{u}) - \nabla p - \beta(\operatorname{div} \boldsymbol{\sigma}_d(\dot{\mathbf{u}}) - \nabla \dot{p}) &= \mathbf{f}, \\ \frac{p}{\kappa} + \operatorname{div} \mathbf{u} &= 0 \end{aligned} \quad \text{in } \Omega. \quad (13)$$

In total, we have thus a system of constrained PDEs, which can also be viewed as a PDAE (partial-differential-algebraic equation). There are several important parameters, among them in particular

- The frequency-dependent damping parameter β . If $\beta = 0$, the term with \dot{p} disappears, and as we will see below, this also affects the index of the semi-discretized system.
- The bulk modulus κ . This parameter governs the term p/κ in the incompressibility constraint. For $\kappa \gg 1$, we obtain a singular perturbation, which in the limit leads to a change of the constraint equation, also affecting the index.

The PDAE (13) still lacks boundary and initial conditions. In practical applications, one deals with mixed Dirichlet and Neumann boundary conditions for the displacement, i.e.,

$$\mathbf{u} = \mathbf{u}_0 \quad \text{on } \Gamma_0, \quad \boldsymbol{\sigma}(\mathbf{u})\mathbf{n} = \boldsymbol{\tau} \quad \text{on } \Gamma_1, \quad (14)$$

where $\partial\Omega = \Gamma_0 \cup \Gamma_1$, \mathbf{u}_0 is a prescribed displacement, $\boldsymbol{\tau}$ a prescribed surface traction, and \mathbf{n} the outer normal vector. Similarly, initial values for the displacements and velocities can be specified. Note that the pressure typically need not be given since it can be determined from the incompressibility constraint.

Extension to Large Deformation and Material Law of Mooney-Rivlin

Finally, we give some comments on how to include finite or large deformations in the model equations and how to introduce appropriate hyperelastic material laws. For better readability, we will mainly use the small displacement case (13) as basic model in the following, but the 2D simulations we will present in the last section are actually based on the hyperelastic material law of Mooney-Rivlin and include large deformations.

For the purpose of modelling large deformation and hyperelastic material laws, it is convenient to use the right Cauchy-Green tensor

$$\mathbf{C} = \mathbf{C}(\mathbf{u}) = (\mathbf{I} + \nabla\mathbf{u})^T(\mathbf{I} + \nabla\mathbf{u}) \quad (15)$$

instead of the linear strain tensor $\boldsymbol{\varepsilon}$ from (1). The first two invariants of this symmetric 3×3 matrix are

$$I_1 = \text{trace } \mathbf{C} = C_{11} + C_{22} + C_{33}, \quad I_2 = \frac{1}{2}(I_1^2 - \text{trace } \mathbf{C}^2).$$

With these quantities, the strain energy function of a material of a Mooney-Rivlin type, which includes rubber-like soft materials, reads [5]

$$W_{\text{MR}} = c_{10}(\bar{I}_1 - 3) + c_{01}(\bar{I}_2 - 3) + \frac{1}{2}\kappa(J - 1)^2 \quad (16)$$

where $J = \det(\mathbf{I} + \nabla\mathbf{u})$, $\bar{I}_1 = I_1 J^{2/3}$, $\bar{I}_2 = I_2 J^{-4/3}$, and c_{10}, c_{01} are material constants. Notice the bulk modulus κ in the last term of (16), which stands for the volume change of the material.

Defining the first Piola-Kirchhoff stress tensor by

$$\mathbf{P}(\mathbf{u}) := \frac{\partial W_{\text{MR}}}{\partial \nabla\mathbf{u}}, \quad (17)$$

the equations of motion in the large-deformation case can be expressed by

$$\rho \ddot{\mathbf{u}}(x, t) = \text{div } \mathbf{P}(\mathbf{u}(x, t)) + \mathbf{f}(x, t) \quad \text{in } \Omega. \quad (18)$$

In comparison to the equations of small deformation (5), the only difference is in the stress tensor \mathbf{P} and its nonlinearity. In a finite element code, the derivatives in (17) are typically computed by symbolic differentiation.

To account additionally for incompressibility, the pressure is related to the volume change through the equation

$$p = -\kappa(J(\mathbf{u}) - 1). \quad (19)$$

Recall that $J(\mathbf{u}) = \det(\mathbf{I} + \nabla \mathbf{u})$, which means that for $J = 1$ we obtain the incompressible case. For a material law of Mooney-Rivlin type, the strain energy function is then replaced by

$$W_{\text{MR}} = c_{10}(\bar{I}_1 - 3) + c_{01}(\bar{I}_2 - 3) - p(J - 1) - \frac{p^2}{2\kappa}. \quad (20)$$

Upon insertion of the pressure from (19), the definition (20) becomes the original strain energy function (16). The first Piola-Kirchhoff stress tensor (17) is now a function $\mathbf{P} = \mathbf{P}(\mathbf{u}, p)$ of both displacement and pressure, and overall we get the equations of motion

$$\begin{aligned} \rho \ddot{\mathbf{u}} - \operatorname{div} \mathbf{P}(\mathbf{u}, p) &= \mathbf{f}, \\ \frac{p}{\kappa} + J(\mathbf{u}) - 1 &= 0 \end{aligned} \quad \text{in } \Omega. \quad (21)$$

Since the determinant J is a nonlinear function of $\nabla \mathbf{u}$, the incompressibility constraint in (21) is nonlinear in general.

Finally, frequency-dependent damping can be included in the large deformation model by using

$$\tilde{\mathbf{P}} = \mathbf{P}(\mathbf{u}, p) + \beta \frac{d}{dt} \mathbf{P}(\mathbf{u}, p)$$

instead of \mathbf{P} . Viscous damping, on the other hand, is introduced in the same way as in the small deformation case. We skip the display of the corresponding PDE system as this provides no further insight.

1.2. Modelling of Microvibrations

Microvibration of skeletal muscle cells is a phenomenon which is related to physiological tremor and which features also similarities to the rhythmic excitation of cardiac cells. The absence of these microvibrations in outer space missions as well as in cancerous tissue indicates their relevance for physiological transport processes in the extracellular matrix structure. Citing from [8,9], we summarize the experimental findings in the following statements:

- *From these results it would appear that a low damped 7-13 Hz resonance process exists in relaxed muscle tissue, which physiologically becomes stimulated by cardiac and muscle forces.*
- *Microvibrations and postural tremor were demonstrated to be strongly influenced by the presence or absence of the earths gravitational field.*

The hypothesis for the vibrational therapy of [21] is that these microvibrations are a pumping mechanism for nutrients. On the other hand, the absence of vibrations leads to malfunctioning and disease. Mechanical stimulation of the diseased muscle tissue in turn leads to a synchronization effect, also called entrainment, that normalizes the cellular rhythmicity and the nutrient flow in the extracellular matrix. This hypothesis suggests that there is a direct link to the mathematical theory of nonlinear oscillators and their synchronous coupling.

A detailed model of the microvibration should be based on specific parameters of the extracellular matrix which interconnects the cells and serves as transport medium for nutrients and by-products. Among these parameters are the temperature, ion concentration, osmolarity, base-acid content, susceptibility, and the dielectricity. However, though nonlinear oscillators are a common phenomenon in biological systems and have been studied at different levels, a physiologically motivated bio-chemical model of this particular process is not known so far. An overview of existing models for cellular rhythms is found in Goldbeter [13].

Instead of tackling the complex bio-chemistry of the extracellular matrix, we concentrate here on the observation that the microvibration leads to a small oscillating displacement of each cell. This displacement can be modelled in a descriptive approach, which results in a simple mechanical model that in future work should be extended to include physiological parameters and reactions. The ultimate goal is to be able to predict the dynamics of vibrational therapies so that the validity of the underlying physiological assumptions can be tested.

Oscillator Model

We consider a one-dimensional chain of N interacting cells. The basic model for the oscillatory motion of each cell is inspired by a mechanical viewpoint and has been studied, among others, by Matthews et al. [20] and Cross et al. [6]. Our oscillator model is given by

$$\ddot{y}_n + \omega_n^2 y_n - \mu(1 - y_n^2)\dot{y}_n + ay_n^3 - D_n \left(\frac{1}{2}(y_{n+1} + y_{n-1}) \right) = 0, \quad (22)$$

where $y_n(t)$ is the displacement of cell n with respect to a reference position. The first three terms of the model form a Van der Pol oscillator with parameter μ while the next term ay_n^3 describes a stiffening of the associated spring, related to a Duffing oscillator. In our computations, we have taken $a = 0$. The last term represents a nearest neighbour coupling between the oscillators, which depends directly on the positions of the neighbours. We set $D_n = D\omega_n$ for the coupling strength, where ω_n is the natural frequency of the n -th oscillator and D a global parameter.

The one-dimensional chain corresponds to an appropriate one-dimensional cross-section through the tissue. A straightforward extension would be to study a two-dimensional array of oscillators, which would lead to a similar set of equations for each oscillator *and* each coordinate direction [7].

One of the objectives of the modeling is to determine whether an externally-driven microvibration applied to the extracellular matrix can cause synchronization of the cellular oscillators. Thus, a measure of synchronization, or coherence, is needed. A commonly used measure of coherence for both mechanical and cellular oscillators is the complex order parameter Ψ

$$\Psi = R \exp^{i\Theta} = \frac{1}{N} \sum_{n=1}^N r_n \exp^{i\theta_n}. \quad (23)$$

In this paper, r_n and θ_n are obtained by local transformation of the position y_n and scaled velocity \dot{y}_n/ω_n of each cell into polar coordinates. We expect that R , which measures in a sense the net strength of the chain of oscillators, may be useful in feedback to the model of the extracellular matrix. However, we are not in a position at the present time to model that feedback, due to a lack of physiological data.

To measure *only* the phase coherence, we form $\chi := \frac{1}{N} \sum_{n=1}^N \exp^{i\theta_n}$ by setting $r_n = 1$ in (23), in which case $R = 1$ represents perfect coherence and $R = 0$ indicates a complete lack of coherence.

1.3. Coupling Macro- and Microscale

We next discuss the coupling of both the PDE model for the muscle tissue and the oscillator chain for microvibrations.

One-way Coupling

In one-way coupling, the motion at the macro-scale is not affected by the microvibrations, which means that the PDE (13) is solved separately and its solution used as input to the oscillator chain. This leads to the question of how to model the coupling via some kind of forcing function.

In our studies, we chose

$$\ddot{y}_n + \omega_n^2 y_n - \mu(1 - y_n^2)\dot{y}_n + ay_n^3 - D_n \left(\frac{1}{2}(y_{n+1} + y_{n-1}) \right) + c(\mathbf{u}) = 0, \quad (24)$$

with an additional periodic internal coupling by taking $D_1(y_2 + y_N)/2$ as coupling term for y_1 and $D_N(y_1 + y_{N-1})/2$ as coupling term for y_N . The forcing function $c(\mathbf{u})$ evaluates the displacement at some point ξ (e.g., a quadrature node) and time t . E.g., a straightforward proportional forcing in the vertical direction reads

$$c(\mathbf{u}) = \gamma \cdot u_y(\xi, t)$$

where u_y is the y -component of the displacement and γ a parameter.

This approach is inspired by the structure of the muscle tissue, which consists of the extracellular matrix and the cells in between. The matrix, a truss-like structure, is mainly composed of collagen and determines the material properties, compare Fig.1. External vibrations will travel through the matrix and reach the cells via the matrix. Due to the tiny length scale at the cell level, the assumption of a simultaneous forcing of a cluster of cells is justified.

Other possible choices are a forcing of the boundary oscillators y_1 and y_N only.

Two-way Coupling

Since we lack a detailed model at the cell level, we only discuss here possible approaches for a two-way coupling. The hypothesis in the vibrational therapy is that the muscle tissue starts to relax when the cells oscillate in a coherent way, which corresponds to a healthy state. In case of no or unsynchronized oscillations, one suspects a hardening effect which makes the tissue stiffer. In our model, this would mean a dependence of material parameters such as the elasticity modulus on the coherence of the microvibrations, i.e.

$$E(x, t) = c(\mathbf{y}, t; x)$$

where $\mathbf{y} = (y_1, \dots, y_N)$ are the oscillators on the microscale around point x .

If one applies the finite element method to discretize the model with such functions for material parameters the integrals in the weak form need to be approximated by appropriate quadrature rules, which means that we require the evaluation of $E(\xi_j, t) = c(\mathbf{y}, t; \xi_j)$ at each quadrature point ξ_j . This coupling mechanism resembles approaches for simulating muscle contraction [11] and is also related to multiscale modelling in the materials sciences.

2. STRUCTURE OF THE SEMIDISCRETIZED EQUATIONS

The PDAE (13) is now discretized in space by applying the finite element method. Due to the mixed formulation, we approximate both the displacement field and the pressure by appropriate basis functions,

$$\mathbf{u}(x, t) \doteq \sum_{i=1}^{n_q} \phi_i(x) q_i(t), \quad p(x, t) \doteq \sum_{j=1}^{n_\lambda} \psi_j(x) \lambda_j(t), \quad (25)$$

with unknown nodal coefficient vectors $\mathbf{q}(t) \in \mathbb{R}^{n_q}$ and $\boldsymbol{\lambda}(t) \in \mathbb{R}^{n_\lambda}$. The structure and the index of the resulting DAE depend on the choice of the basis functions ϕ_i and ψ_j and on the material parameters, in particular the bulk modulus κ and the damping coefficient β .

2.1. Structure of Matrices and Full Rank Criterion

We skip the display of the weak form of (13) and proceed directly with the DAE that results from the finite element approximation (25). This DAE can be written as

$$\begin{aligned} \mathbf{M}\ddot{\mathbf{q}} + \mathbf{A}\mathbf{q} + \mathbf{B}^T\boldsymbol{\lambda} + \mathbf{D}\dot{\mathbf{q}} + \beta\mathbf{B}^T\dot{\boldsymbol{\lambda}} &= \mathbf{f}(t), \\ -\frac{1}{\kappa}\mathbf{M}_p\boldsymbol{\lambda} + \mathbf{B}\mathbf{q} &= \mathbf{0}. \end{aligned} \quad (26)$$

Here,

$$\mathbf{M} := \left(\int_{\Omega} \rho \phi_i(x)^T \phi_j(x) dx \right)_{i,j=1:n_q} \quad \text{and} \quad \mathbf{M}_p := \left(\int_{\Omega} \psi_i(x) \psi_j(x) dx \right)_{i,j=1:n_\lambda}$$

are the mass matrices for displacement and pressure, respectively. The stiffness matrix is given by

$$\mathbf{A} := \left(\int_{\Omega} \boldsymbol{\sigma}_d(\phi_i(x)) : \boldsymbol{\varepsilon}(\phi_j(x)) dx, \right)_{i,j=1:n_q},$$

while the constraint matrix is obtained from

$$\mathbf{B}^T := \left(\int_{\Omega} \operatorname{div} \varphi_i(x) \cdot \psi_j(x) dx \right)_{i=1:n_q, j=1:n_\lambda}.$$

Finally, the damping matrix is a simple linear combination $\mathbf{D} = \alpha \mathbf{M} + \beta \mathbf{A}$.

For standard finite elements, the mass matrices for displacement and pressure are symmetric positive definite while the stiffness matrix is positive semi-definite. Of particular interest is the $n_\lambda \times n_q$ constraint matrix \mathbf{B} , as we require it below to be of full rank. Clearly, the dimension n_λ of the constraints must be less than the dimension of the displacement variables n_q .

We can express the full rank requirement in terms of the singular values of \mathbf{B} , which are given by the singular value decomposition [12, §2.5]

$$\mathbf{U}^T \mathbf{B} \mathbf{V} = \operatorname{diag}(\sigma_1, \dots, \sigma_{n_\lambda}) \in \mathbb{R}^{n_\lambda \times n_q}$$

with orthogonal matrices $\mathbf{U} \in \mathbb{R}^{n_\lambda \times n_\lambda}$ and $\mathbf{V} \in \mathbb{R}^{n_q \times n_q}$. The singular values are ordered as

$$\sigma_1 \geq \sigma_2 \geq \dots \geq \sigma_{n_\lambda} \geq 0,$$

and for the full rank of \mathbf{B} we require $\sigma_{\min} := \sigma_{n_\lambda} > 0$. Observe that

$$\frac{\boldsymbol{\lambda}^T \mathbf{B} \mathbf{B}^T \boldsymbol{\lambda}}{\boldsymbol{\lambda}^T \boldsymbol{\lambda}} = \frac{\boldsymbol{\tau}^T \operatorname{diag}(\sigma_1^2, \dots, \sigma_{\min}^2) \boldsymbol{\tau}}{\boldsymbol{\tau}^T \boldsymbol{\tau}} \geq \sigma_{\min}^2$$

for $\boldsymbol{\lambda} \neq \mathbf{0}$ and $\boldsymbol{\tau} := \mathbf{U}^T \boldsymbol{\lambda}$. In case of $\boldsymbol{\tau} = (0, \dots, 0, 1)^T \in \mathbb{R}^{n_\lambda}$, this inequality is sharp and we conclude

$$\sigma_{\min}^2 = \min_{\boldsymbol{\lambda}} \frac{\boldsymbol{\lambda}^T \mathbf{B} \mathbf{B}^T \boldsymbol{\lambda}}{\boldsymbol{\lambda}^T \boldsymbol{\lambda}} \iff \sigma_{\min} = \min_{\boldsymbol{\lambda}} \frac{\|\mathbf{B}^T \boldsymbol{\lambda}\|_2}{\|\boldsymbol{\lambda}\|_2}.$$

Moreover, using the definition of the operator norm we get the identity

$$\|\mathbf{B}^T \boldsymbol{\lambda}\|_2 = \max_{\mathbf{v}} \frac{\|\mathbf{v}^T \mathbf{B}^T \boldsymbol{\lambda}\|_2}{\|\mathbf{v}\|_2} = \max_{\mathbf{v}} \frac{\boldsymbol{\lambda}^T \mathbf{B} \mathbf{v}}{\|\mathbf{v}\|_2}$$

since $\|\mathbf{v}^T \mathbf{B}^T \boldsymbol{\lambda}\|_2 = |\boldsymbol{\lambda}^T \mathbf{B} \mathbf{v}|$. Overall, we have thus derived the minimax characterization [22]

$$\min_{\boldsymbol{\lambda}} \max_{\mathbf{v}} \frac{\boldsymbol{\lambda}^T \mathbf{B} \mathbf{v}}{\|\boldsymbol{\lambda}\|_2 \|\mathbf{v}\|_2} = \sigma_{\min}(\mathbf{B}) > 0 \tag{27}$$

as equivalent to the full rank criterion. It is important to realize that (27) is nothing else than the discrete inf-sup condition of mixed and hybrid finite element analysis [4]. If the basis functions ϕ_i and ψ_j in (25) satisfy the inf-sup condition, i.e., they are "well-balanced" in the finite element sense, then the full rank of the constraint matrix \mathbf{B} is guaranteed. In our specific application, the Taylor-Hood "P2-P1" combination with quadratics for the displacements and linears for the pressure is well-known to be a stable pairing for which the inf-sup condition holds.

2.2. Index of Semi-discretized Equations

We begin with the small-deformation case, which after semi-discretization yields the DAE (26), assuming the full rank condition (27) for the constraint matrix \mathbf{B} to hold. The semi-explicit structure of the equations simplifies the analysis greatly, and we can draw on well-known results from the field of mechanical multibody systems, which basically lead to the same structure [22].

Case $\kappa = \infty$: In the purely incompressible case, the term $\kappa^{-1}M_p\lambda$ in the constraint equation disappears. If additionally $\beta = 0$, the equations (26) have exactly the same structure as in multibody dynamics, and accordingly the index is three. However, for frequency-dependent damping with $\beta > 0$, the index drops to two since the term $\beta B^T \dot{\lambda}$ in the dynamic equations reduces the number of differentiation steps that are necessary to generate an ODE for λ by one.

Case $\kappa < \infty$: For finite bulk modulus, the constraint equation can be rewritten as

$$M_p\lambda = \kappa Bq.$$

As the mass matrix for the pressure is invertible, we can thus directly solve for $\lambda = \lambda(q)$, which means that the index amounts to one in this case, regardless of the damping parameter β . Though this seems a favorable situation, one should be careful here as a large value of κ leads to a singularly perturbed system that is close to a higher index system. Depending on the tolerances and norms used, the time integration will reflect that closeness or not.

From a physical point of view, we note that deformable solids always exhibit some frequency-dependent damping. Moreover, muscle tissue is not fully incompressible, and accordingly, in practical simulations one will typically use a finite bulk modulus κ and a damping parameter $\beta > 0$. Thus the regularization has a solid physical basis.

Next, we turn to the large deformation case (21), where the semi-discretization by finite elements introduces additional nonlinearities. We summarize here the structure of the resulting equations as they are generated in the COMSOL package [5]. COMSOL utilizes velocity variables $v = \dot{q}$ to obtain a first order system, which in the case $\beta = 0$ reads

$$\begin{aligned} \dot{q} &= v, \\ M\dot{v} &= f_a(q, \lambda) - \alpha Mv + f_c(t), \\ 0 &= -\frac{1}{\kappa}M_p\lambda + j(q). \end{aligned} \quad (28)$$

Here, the force term f_a is the discretized analogue of the Piola-Kirchhoff stress tensor $P(u, p)$, the function $j(q)$ corresponds to the determinant $J(u) - 1$ in (21), and f_c is the load vector.

If frequency-dependent damping is included, i.e., $\beta > 0$, COMSOL treats the derivative $\dot{\lambda}$ as an additional unknown μ , which results in an extended system

$$\begin{aligned} \dot{q} &= v, \\ \dot{\lambda} &= \mu, \\ M\dot{v} &= f_a(q, \lambda) - \alpha Mv + \beta f_b(q, v, \mu) + f_c(t), \\ 0 &= -\frac{1}{\kappa}M_p\lambda + j(q), \end{aligned} \quad (29)$$

where f_b corresponds to the evaluation of $\frac{d}{dt}P(u, p)$.

With respect to the index, the two DAEs (28) and (29) require a separate discussion.

Case $\beta = 0$ and formulation (28): An appropriate linearization reduces (28) to the linear DAE (26) with $\beta = 0$, which means that the index analysis from above remains valid. For bulk modulus $\kappa = \infty$, the index is three, otherwise one.

Case $\beta > 0$ and formulation (29): Upon linearization of (29) we obtain

$$\begin{aligned} \dot{q} &= v, \\ \dot{\lambda} &= \mu, \\ M\dot{v} &= -Aq - B^T\lambda - Dv - \beta B^T\mu + f(t), \\ 0 &= -\frac{1}{\kappa}M_p\lambda + Bq. \end{aligned} \quad (30)$$

For finite bulk modulus $\kappa < \infty$, we perform one differentiation step for the constraint and get

$$M_p\dot{\lambda} = M_p\mu = \kappa Bv.$$

DAE	κ	β	Index
(26)	∞	0	3
(26)	$< \infty$	0	1
(26)	∞	> 0	2
(26)	$< \infty$	> 0	1
(28)	∞	0	3
(28)	$< \infty$	0	1
(29)	∞	> 0	3
(29)	$< \infty$	> 0	2

TABLE 1. Dependence of the index on the formulation and the parameters. We note that (26) corresponds to the small-deformation model, whereas (28) and (29) correspond to the large-deformation model.

The extra multiplier $\boldsymbol{\mu}$ requires now a second differentiation to generate an ODE, and the index of the system is two. However, note that the original multiplier $\boldsymbol{\lambda}$ is still an index-one variable. A similar argumentation for $\kappa = \infty$ shows that the index is three in that case, with $\boldsymbol{\mu}$ as index-three variable and $\boldsymbol{\lambda}$ as index-two variable. To summarize, the introduction of the additional multiplier $\boldsymbol{\mu}$ and the corresponding differentiation in (29) raise the index by one. Table 1 gives a compilation of these findings. It is interesting to note that in the limit as $\kappa \rightarrow \infty$ and $\beta \rightarrow 0$, the index of (29) is four. In the next section, we will present statistics of simulation runs by DASPK [3] for the different cases and discuss how the time integration is actually affected.

The practical question is: how should we formulate the DAE for efficient and reliable numerical solution? It is common knowledge in DAEs that there are some formidable difficulties in treating higher-index systems directly. Systems of index one, and to some extent also semi-explicit systems of index two, however, can be solved by methods such as the BDF [2].

As seen above, regularization with physically meaningful values of κ and β lowers the index. There is some cause for concern about relying on the regularization to reduce the index, however, because it is possible that the DAE solver will struggle with the regularized system for basically the same reasons that it fails for the limiting higher-index system.

Another possibility is to reduce the index by differentiating the constraints. Omitting the damping terms in the linearized equations (26), this results in

$$\begin{aligned} M\ddot{\mathbf{q}} + \mathbf{A}\dot{\mathbf{q}} + \mathbf{B}^T\boldsymbol{\lambda} &= \mathbf{f}, \\ \mathbf{B}\dot{\mathbf{q}} &= \mathbf{0}, \end{aligned} \quad (31)$$

which is of index two. Due to the differentiation, we lose the information of the original constraint, which is negligible as long as the constraints are linear, but will lead to some drift away from the constraints in the large-deformation case.

When using a sophisticated finite element package such as COMSOL for the generation of the matrices and the evaluation of the semidiscretized equations, it is usually very difficult or even impossible to intervene in order to set up an index-reduced formulation such as (31) and pass it to the time integrator. It thus seems a natural idea to introduce the new formulation already at the PDE level and to let the finite element solver take care of the remaining steps. A PDE model that corresponds to the index-two system (31) reads

$$\begin{aligned} \rho\ddot{\mathbf{u}} - \operatorname{div} \boldsymbol{\sigma}_d(\mathbf{u}) - \nabla p &= \mathbf{f}, \\ \operatorname{div} \dot{\mathbf{u}} &= 0 \end{aligned} \quad \text{in } \Omega. \quad (32)$$

In the next section, we will compare the nonlinear analogue of (32) with the results obtained by the regularized formulations.

Finally, one might reasonably wonder, why not consider a stabilized index-reduction such as that described in [10], which eliminates the possibility of drift away from the original constraint. For (31), this leads to

$$\begin{aligned} M\dot{\mathbf{q}} &= M\mathbf{q} - \mathbf{B}^T \boldsymbol{\mu}, \\ M\dot{\mathbf{v}} &= \mathbf{f} - \mathbf{A}\mathbf{q} - \mathbf{B}^T \boldsymbol{\lambda}, \\ \mathbf{0} &= \mathbf{B}\mathbf{q}, \\ \mathbf{0} &= \mathbf{B}\mathbf{v}. \end{aligned} \tag{33}$$

This formulation is based on a transformation to first order with velocity variables \mathbf{v} , in combination with additional constraints on the velocity level and corresponding multipliers $\boldsymbol{\mu}$. It is easy to show that $\boldsymbol{\mu} = \mathbf{0}$ for the exact solution and that the index of (33) is two. The stabilized formulation (33) corresponds to the PDE

$$\begin{aligned} \rho\dot{\mathbf{u}} &= \rho\mathbf{w} + \nabla r, \\ \rho\dot{\mathbf{w}} - \mathbf{div} \boldsymbol{\sigma}_d(\mathbf{u}) - \nabla p &= \mathbf{f}, \\ \mathbf{div} \mathbf{w} &= 0, \\ \mathbf{div} \mathbf{u} &= 0, \end{aligned} \quad \text{in } \Omega \tag{34}$$

with extra pressure variable r . Assuming sufficient smoothness, we then have

$$0 = \mathbf{div} \mathbf{w} = \mathbf{div} \dot{\mathbf{u}} - \frac{1}{\rho} \mathbf{div} \nabla r = \frac{1}{\rho} \Delta r.$$

The desired conclusion $r = 0$ is obviously not straightforward and requires additional information such as boundary conditions, which gives a hint that the stabilization at the PDE level is not as easy as it seems.

The stabilized PDAE (34) can be directly specified in COMSOL using the multiphysics mode to define the extra variables and the "Weak Form" option to define the equations. However, in our tests the discretization did not yield a system of exactly the form (33) but with a different constraint matrix $\tilde{\mathbf{B}} \neq \mathbf{B}$ for the extra multiplier $\boldsymbol{\mu}$. This was due to the fact that COMSOL discretizes the extra multiplier using quadratic finite elements, while the original multiplier is treated by linear finite elements. Thus the additional multiplier $\boldsymbol{\mu}$ is not uniquely zero, and in fact this approach yields an incorrect solution. We were not able, using COMSOL defaults, to change the discretization of r to a linear ansatz.

3. COMPUTATIONAL RESULTS

In this section, we report on the simulations that were performed. We start with a study of the oscillator chain in a simplified setting and then continue with a 2D model for the muscle tissue that was solved by means of COMSOL and DASPK [3].

3.1. Oscillator Chain

In order to observe a synchronization process, it is usually necessary to perform long-time simulations over many periods of oscillation. Since this is rather costly in combination with a two-dimensional finite element model, we first developed a simplified one-dimensional model for the macroscale that is based on the linear damped wave equation

$$\rho(\ddot{u}(x, t) + \alpha\dot{u}(x, t)) = EAu_{xx}(x, t) + \beta EA\dot{u}_{xx}(x, t). \tag{35}$$

Here, $u(x, t)$ is the longitudinal displacement of a thin rod of length L , E the elasticity modulus, A the cross section area, and ρ the mass density. As boundary conditions, we consider a fixed left end where $u(0, t) = 0$ and a right end subject to an external load, $u_x(L, t) = \tau(t)$ with $\tau(t)$ being a sinusoidal signal oscillating at 8 Hz. This signal travels through the rod and thus reaches all material points. The displacement $u(L/2)$ of the midpoint serves as input to the term $c(u)$ in the one-way coupling (24). Thus we investigate a single representative area of the tissue around the midpoint and use there the oscillator chain as a refined model.

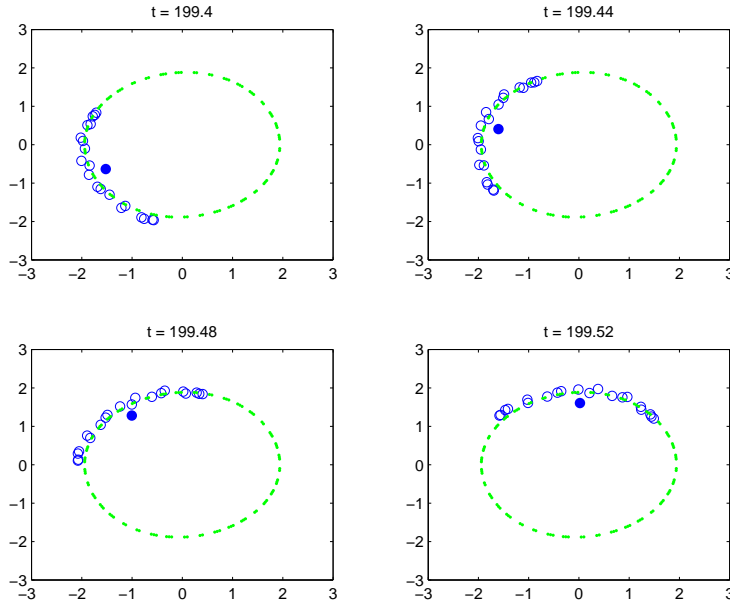


FIGURE 2. Snapshots of the positions of 20 oscillators in the complex plane. Each circle denotes one oscillator. The big dot is the common centroid.

The discretization of (35) by linear finite elements results in a system of second order ODEs

$$M\ddot{q} + A\dot{q} + Dq = f(t) \quad (36)$$

that can be integrated by standard MATLAB solvers such as `ode15s`. Simultaneously, the oscillator equations (24) are integrated and the coherence measure (23) is computed at each timestep. In the beginning, the system is assumed to be at rest, which means that zero initial values for the displacements and for the oscillators are chosen. The sinusoidal input signal $\tau(t)$ is then slowly increased by means of a shifted sigmoid function.

The following data (in dimensionless form) were used to generate the solutions displayed in Figs. 2 and 3. The material parameters are $EA = 1.E6$, $\rho = 1.E3$, $L = 0.1$, $\alpha = 0.25$, $\beta = 0.001$, and 10 finite elements were applied. For the oscillator model, the basic frequency was set to $\omega_n = 16\pi + \xi_n$ with ξ_n being a random number in the interval $[-0.05, 0.05]$, generated by MATLAB's `rand` command. The Van der Pol parameter was set to $\mu = 2$ for all oscillators, the cubic Duffing term disabled, and the coupling to the nearest neighbours enforced by $D_n = D \cdot \omega_n$ with $D = 3$. The simulation interval was $[0, 200]$.

For $N = 20$ coupled oscillators, Fig. 2 shows the synchronization that can be observed. By transformation of the position y_n and the scaled velocity \dot{y}_n/ω_n of each oscillator into polar coordinates and marking their position in the complex plane, one gets an impression how the oscillators travel in a group clockwise around the origin. The extra marker stands for the position of the coherence parameter Ψ from (23), which is the common centroid of the oscillators. The synchronization is strong, but not optimal, which can be seen in Fig. 3. After the initial acceleration phase due to the sigmoid function, the absolute value $|\Psi|$ decreases according to the different natural frequencies, and later the nonlinear synchronization comes into play and reaches a constant level. In the complex plane, the values of Ψ first spiral outwards from the origin and later on travel around it.

We remark that the degree of synchronization depends strongly on the chosen data. E.g., selecting a wider range of natural frequencies or a smaller coupling parameter D will lead to a smaller coherence.

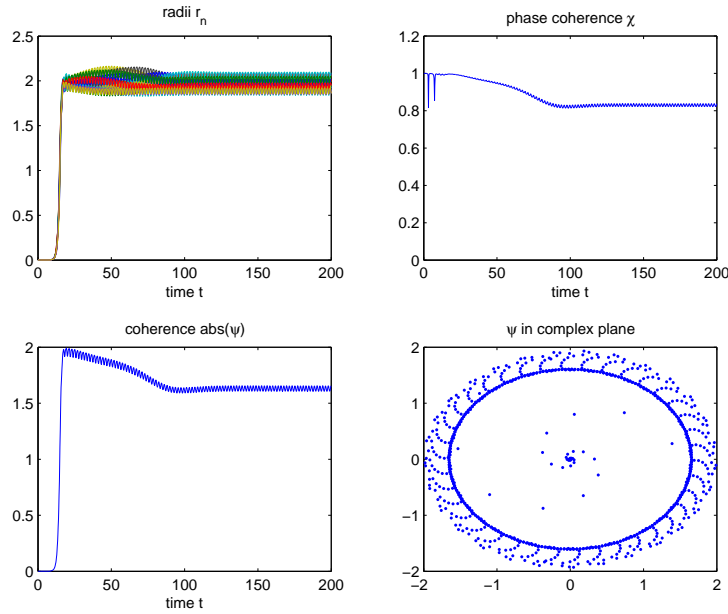
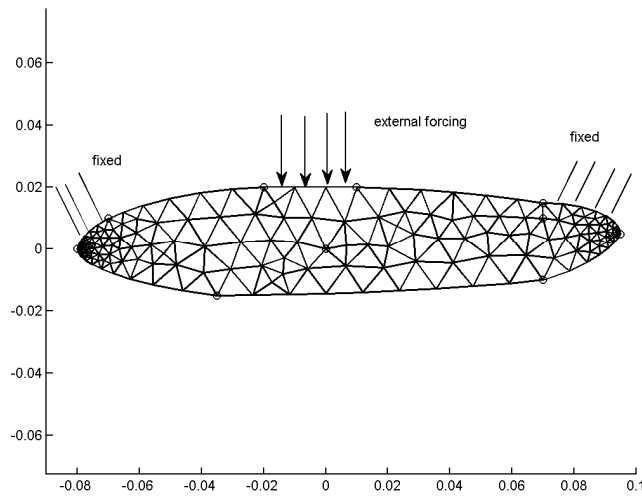
FIGURE 3. Radii r_n and evolving coherence Ψ of the oscillators

FIGURE 4. Finite element mesh and boundary conditions.

3.2. Two-dimensional Model

The geometry of the two-dimensional model is displayed in Fig. 4, along with the finite element mesh generated by COMSOL. As boundary conditions (14), two segments at both ends are kept fixed with zero displacement, and in the middle a surface load $\tau(t) = (0, \tau_y(t))$ is applied in the vertical direction, with $\tau_y(t)$ being again a sinusoidal signal oscillating at 8 Hz. For a refined model including a surface load that mimicks the vibrational therapy of [21] and modified boundary conditions for the tendons see [24].

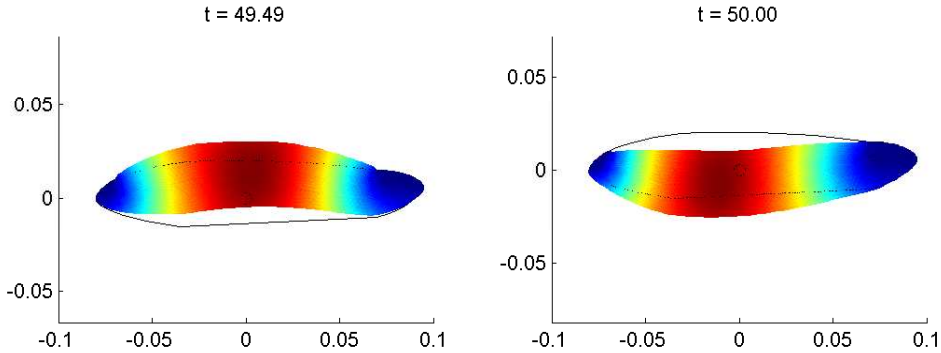


FIGURE 5. Two snapshots of the deformed muscle.

We used $\rho = 1.1E3$, $\alpha = 1$, $c_{10} = 1.E4$, and $c_{01} = 2.E2$ as parameters for the simulation runs, which are typical values for muscle tissue. For the finite element discretization, we took the default "P2-P1" mode, which means quadratics for the displacements and linears for the pressure. In total, this gives 1545 unknowns \mathbf{q} and $\boldsymbol{\lambda}$ in the DAE (29). As above, the system is first assumed to be at rest, which means zero initial values for the displacements, the pressure and the oscillators. The sinusoidal input signal is then slowly introduced by means of a shifted sigmoid function, i.e., $\tau_y(t) = 100 \cdot (1/(1 + \exp(-10t + 8)) - 1/(1 + \exp(8))) \sin(16\pi t)$.

The snapshots of Fig. 5 showing the scaled deformation of the muscle are taken from a simulation interval $[t_0, t_{\text{end}}] = [0, 50]$. After an initial phase, the muscle oscillates synchronously with the surface load, which can be observed in Fig. 6. It contains the vertical displacement of the origin $(0, 0)$ over the last three seconds.

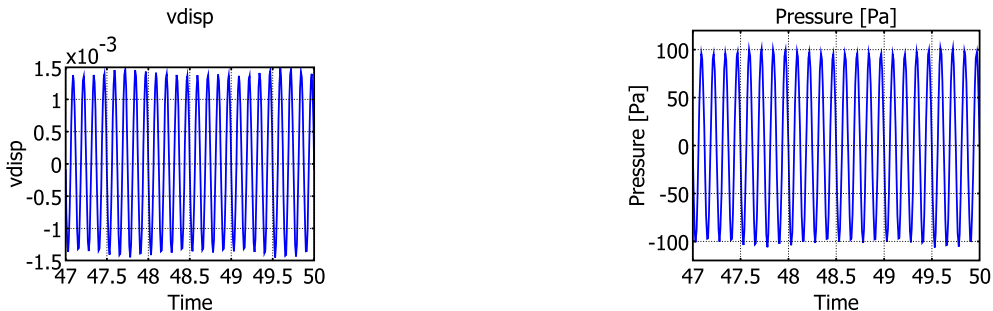
We next discuss the performance of the time integrator DASPK for the different formulations introduced in Section 2. When solving a DAE in COMSOL, it is possible to activate a checkbox that excludes the algebraic variables from the stepsize control, which is important for problems of higher index. In all the runs to be discussed below, the checkbox was activated. For a shorter integration interval $[0, 10]$, relative tolerance 1.E-3 and absolute tolerances 1.E-5 (displacements) and 1.E-1 (pressure), the time integration yields the statistics summarized in Table 2. Since we analyze several formulations with different physical parameters, there is no reference solution available, but we remark that all the runs gave comparable results.

The case $\kappa < \infty, \beta = 0$ corresponds to (28) and yields a system of index one. As expected, the performance of DASPK is very good with relatively few (approximately 2%) rejected steps. Adding frequency-dependent damping ($\beta > 0$) raises the index by one, but is actually beneficial with respect to the number of steps and the number of rejected steps. In part, this behavior can be explained by reconsidering (29) where the additional multiplier $\boldsymbol{\mu}$ is the only index-two variable, and this variable is excluded from the stepsize control.

The case $\kappa = \infty, \beta > 0$ leads to a DAE of index three, but again, in (29) the additional multiplier $\boldsymbol{\mu}$ is the only index-three variable, and this variable is excluded from the stepsize control. In accordance with that, the statistics are still satisfactory. Finally, the fully incompressible case $\kappa = \infty$ with zero frequency-dependent damping $\beta = 0$, which is also index three, leads to an unsuccessful termination after repeated failures of Newton's method. Here, the pressure λ is an index-three variable that, using COMSOL defaults, cannot be excluded from the stepsize control. We remark that a test run with the nonlinear analogue of the index-two formulation (31) and $\kappa = \infty, \beta = 0$ gave also satisfactory results with 3384 steps in total and 62 rejected steps.

Overall, the regularization with both finite bulk modulus and frequency-dependent damping is the most promising approach in this example, but all other formulations except the index-three case with $\kappa = \infty, \beta = 0$ performed satisfactorily as well.

Finally, an example of the one-way coupling with the oscillator chain (24) is presented in Fig. 7. The one-way coupling was implemented in COMSOL using the "Global Equations" option, which leads to an additional system of ODEs that is solved simultaneously with the DAE (29) by DASPK. As forcing for the oscillators, we used the vertical displacement of the origin displayed in Fig. 6.

FIGURE 6. Vertical displacement and pressure in the origin $(0, 0)$.

DAE	κ	β	Index	# steps	# NRJ	# NCF
(28)	1.E5	0	1	3275	76	0
(29)	1.E5	0.0001	2	2765	64	0
(29)	∞	0.0001	3	3374	69	0
(28)	∞	0	3	362-terminated	26	10

TABLE 2. Statistics data from COMSOL runs. NRJ = Number of rejected steps, NCF = Number of convergence failures

In this example, we set $N = 5$ for the oscillators and again varied the basic frequency via $\omega_n = 16\pi + \xi_n$ with ξ_n being a random number in the interval $[-0.5, 0.5]$. The Van der Pol parameter was set to $\mu = 2$ for all oscillators, the cubic Duffing term disabled, and the coupling to the nearest neighbours enforced by $D_n = D \cdot \omega_n$ with $D = 3$. The simulation interval was $[0, 50]$. As can be observed in Fig. 7, the synchronization shows a behavior similar to that of the one-dimensional case.

Since the plots in this section contain mainly static information and only partially reflect the dynamics of the system, we also generated several animations that illustrate the model and that are available for download at the website [23]. The movie named `musclemovie` is an animation of the two-dimensional muscle model, showing the total deformation and how the external excitation acts on the structure, cf. Fig. 5. The movie `musclehardening` contains a refined simulation of [24] where the material parameters of the muscle were changed in a region in the interior. In this way, hardening of muscle tissue and the effect of incoming waves from the excitation can be analysed. The last movie `chainmovie` is an animation of the snapshots presented in Fig. 2 and shows how the oscillators travel in a group in the complex plane.

4. CONCLUSIONS AND OUTLOOK

In this work, we have developed a model for the passive behavior of skeletal muscle tissue including mechanical microvibrations at the cell level. With respect to the model, we were able to verify the synchronization at the micro-scale based on one-way coupling with a finite element simulation at the macro-scale. This supports the underlying hypothesis of vibrational therapies that cellular rhythmicity can be stimulated by external excitation. What still needs to be developed is a more detailed model of the extracellular matrix, which interconnects the cells and serves as transport medium for nutrients and waste products.

With respect to numerical analysis, we have seen that incompressible or nearly incompressible solids lead to an intricate PDAE, whose index, after semi-discretization in space by mixed finite elements, depends on two specific parameters, the bulk modulus and the amount of frequency-dependent damping. For physically meaningful values of the parameters, which correspond to a system of index one, the time integration by DASSP performed best, but even for the limit cases that correspond to higher index formulations, the performance was

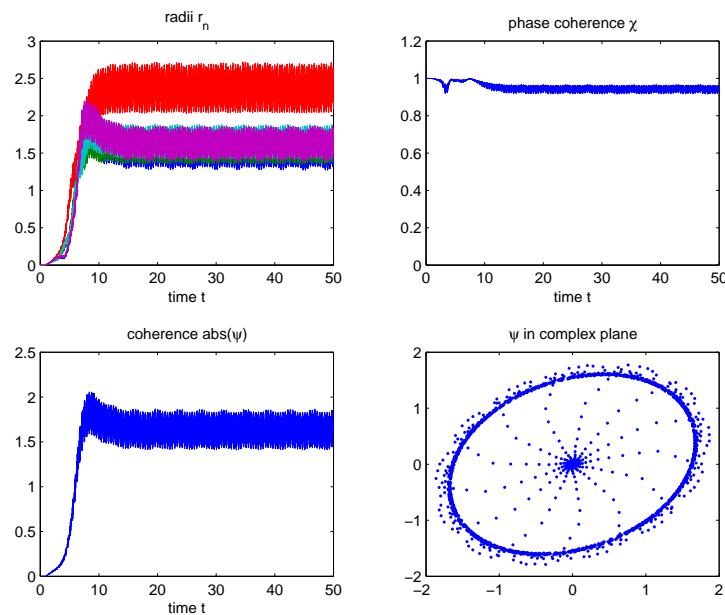


FIGURE 7. One-way coupling with phase coherence χ and coherence Ψ .

satisfactory. The only exception is the pure index-three case with infinite bulk modulus and vanishing damping parameter. In this context, the stabilization (34) should be further investigated, as well as the apparently stabilizing role of the damping parameter.

Finally, using COMSOL as computational platform gives us the ability to extend the model towards an incorporation of greater physical or physiological details.

Acknowledgements

We gratefully acknowledge the work of S. Thiemann and F. Dietrich on earlier versions of the tissue and the oscillator model. Furthermore, we thank U. Randoll for initiating this investigation at the interface between mathematics, computer science and medical research. J. Ystrom of COMSOL AB gave us also valuable hints on specific implementation details.

REFERENCES

- [1] Ascher, U., Petzold, L.: *Computer Methods for Ordinary Differential Equations and Differential-Algebraic Equations*. SIAM 1998
- [2] Brenan, K.E., Campbell, S.L., Petzold, L.R.: *The Numerical Solution of Initial Value Problems in Ordinary Differential-Algebraic Equations*. SIAM 1996
- [3] Brown, P., Hindmarsh, A., Petzold, L.R.: *Using Krylow methods in the solution of large-scale differential-algebraic systems*. SIAM J. Sci. Comp. 15(6), 1467-1488 (1994)
- [4] Brezzi, F., Fortin, M.: *Mixed and Hybrid Finite Element Methods*. Springer 1991
- [5] COMSOL Multiphysics User Manual, Version 3.4, 2007
- [6] Cross, M., Rogers, J., Lifshitz, R., Zumdieck, A.: *Synchronization by reactive coupling and nonlinear frequency pulling*. Physical Review E 73 (2006)
- [7] Dietrich, F.: *Ein Zweiskalenansatz zur Modellierung der Skelettmuskulatur*. Diploma Thesis TU München, 2007
- [8] Gallasch, E.; Moser, M.: *Effects of an eight-day space flight on microvibration and physiological tremor*. Am. J. Physiol. 273, R86-92 (1997)
- [9] Gallasch, E.; Kenner, T.: *Characterisation of arm microvibration recorded on an accelerometer*. Eur. J. Appl. Physiol. 75: 226-232 (1997)

- [10] Gear, C., Gupta, G., Leimkuhler, B.: *Automatic Integration of the Euler-Lagrange Equations with Constraints*. J Comp Appl Math 12:77-90 (1985)
- [11] Gielen, A., Oomens, C., Bovendeerd, P., Arts, T.: *A Finite Element Approach for Skeletal Muscle using a Distributed Moment Model of Contraction*. Comput Methods Biomech Biomed Engin 231-244 (2000)
- [12] Golub, G., van Loan, C.: *Matrix Computations*. 3rd ed., John Hopkins University Press, Baltimore, 1996
- [13] Goldbeter, A.: *Biochemical Oscillations and Cellular Rhythms*. Cambridge University Press, 1996
- [14] Hill, A.V.: *The Heat of Shortening and the Dynamic Constants of Muscle*. Proceedings of the Royal Society of London. Series B, 1938
- [15] Hughes, T.J.: *The Finite Element Method*. Prentice Hall, Englewood Cliffs, 1987
- [16] Huxley, A.F.: *Muscle structure and theories of contraction*. Prog Biophys Biophys Chem 7:255-318 (1957)
- [17] J. Sundnes, G. T. Lines, and A. Tveito: *An operator splitting method for solving the Bidomain equations coupled to a volume conductor model for the torso*. Mathematical biosciences 194(2):233-248 (2005)
- [18] Maurel, W., Y Wu, N., Thalmann, D.: *Biomechanical models for soft tissue simulation*. Springer, 1998
- [19] Marsden, J.E., Hughes, T.J.R.: *Mathematical Foundations of Elasticity*. Dover Publications, 1994
- [20] Matthews, P., Mirollo, R., Strogatz, St.: *Dynamics of a large system of coupled nonlinear oscillators*. Physica D 52, 293-331 (1991)
- [21] Randoll, U.: *Matrix-Rhythm-Therapy of Dynamic Illnesses*. In: Heine, H., Rimpler M.,(eds.) *Extracellular Matrix and Groundregulation System in Health and Disease*. G. Fischer, Stuttgart Jena New York, pp. 57-70, 1997
- [22] Simeon, B.: *On Lagrange multipliers in flexible multibody dynamics*. Comp.Meth.Appl.Mech.Engnrg. 195:6993-7005 (2006)
- [23] www-m2.ma.tum.de/~simeon/m2an
- [24] Thiemann, S.: *Modellierung und numerische Simulation der Skelettmuskulatur*. Diploma thesis, TU München 2006
- [25] Zahalak, G.I., Motabarzadeh, I.: *A re-examination of calcium activation in the Huxley cross-bridge model*. J. Biomech. Engng 119:20-29 (1997)